IL NUOVO CIMENTO **46 C** (2023) 20
DOI 10.1393/ncc/i2023-23020-3

Colloquia: La Thuile 2022

ttX and top properties in ATLAS and CMS

Barbara Alvarez Gonzalez
on behalf of the ATLAS and CMS Collaborations
University of Oviedo and ICTEA - Oviedo, Spain

received 19 September 2022

Summary. — The top quark offers a very rich physics program. This talk focuses on searches for flavor-changing neutral-current (FCNC) and on measurements and searches for rare top quark production modes, the so called ttX processes where X is a boson ($W^{\pm}$, Z, γ or H). FCNC couplings are strongly suppressed in the standard model (SM) but included in many extensions of the SM. The ttX processes become fully accessible with the Run 2 data inclusively and differentially and first searches are carried out within the framework of an effective field theory. The measurements and searches presented are performed with the full Run 2 data of the CERN Large Hadron Collider (LHC) at a center-of-mass of 13 TeV with the ATLAS (*JINST*, **3** (2008) S08003) and CMS (*JINST*, **3** (2008) S08004) experiments.

1. – Search for FCNC couplings between the top-quark and the photon with the ATLAS detector

The analysis uses data collected in proton-proton (pp) collisions during the LHC Run 2 corresponding to an integrated luminosity of 139 fb^{-1} [1]. The final state consists of a charged lepton, missing transverse momentum, a b-tagged jet, one high momentum photon and possibly additional jets. The main background contributions are: $t\bar{t}\gamma$, Wγ+jets and fakes. Backgrounds with prompt photons are modelled by Monte Carlo (MC) simulation and there are dedicated control regions which are included in the final fit to extract the background normalization. Fakes either from electrons or hadrons are modelled from MC but corrected with data-driven scale factors.

A multiclass deep neural network (DNN) is used to classify events as either one of the two signal categories, both FCNC top-quark production and decay are considered, or as background as shown in fig. 1.

No significant excess of events over the background prediction is observed and 95% confidence level (CL) upper limits on the strength of left- and right-handed FCNC interactions are set. The 95% CL bounds on the branching fractions (BRs) for the

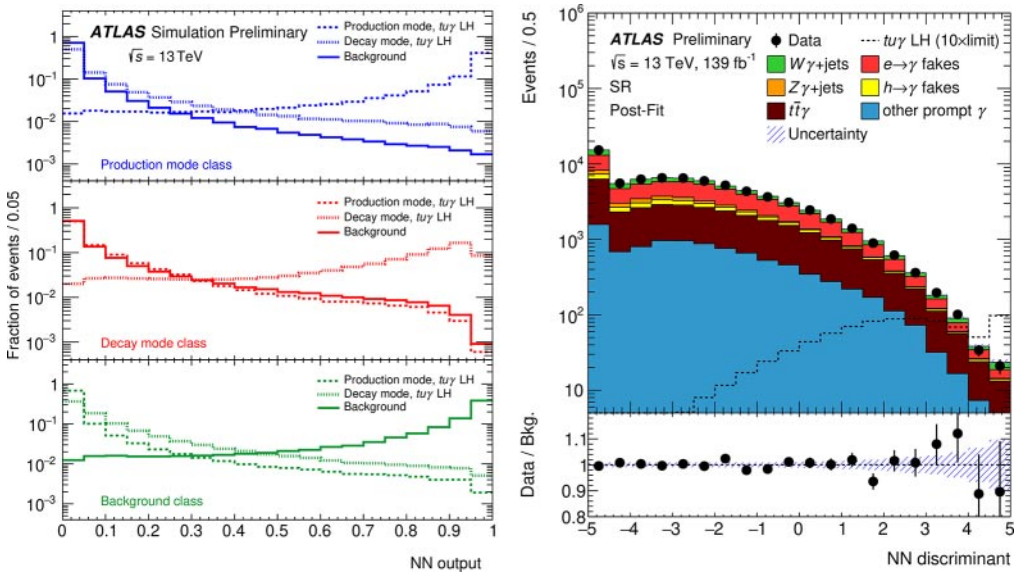

Fig. 1. – Left: The classifier output of the multiclass Neural Network (NN) for the tuγ LH coupling. The output of the FCNC production mode class is shown in blue (top), the output of the FCNC decay mode class is shown in red (middle) and the output of the SM background class is shown in green (bottom). Right: Post-fit distributions of a background-only fit to the NN discriminant in the SR for the tuγ coupling [1].

FCNC top-quark decays, estimated from both top-quark production and decay, are BR(t$\to$uγ)$< 0.85 \times 10^{-5}$ and BR(t$\to$cγ)$< 4.2 \times 10^{-5}$ for a left-handed tqγ coupling, and BR(t$\to$uγ)$< 1.2 \times 10^{-5}$ and BR(t$\to$cγ)$< 4.5 \times 10^{-5}$ for a right-handed coupling.

2. – Search for FCNC interactions of a top quark and a gluon in pp collisions with the ATLAS detector

A search with data corresponding to an integrated luminosity of 139 fb^{-1} is presented for the production of a single top quark via left-handed flavour-changing neutral-current interactions of a top quark, a gluon and an up or charm quark [2]. The leading-order Feynman diagram is shown in fig. 2. Events with exactly one electron or muon, exactly one b-tagged jet and missing transverse momentum are selected, resembling the decay

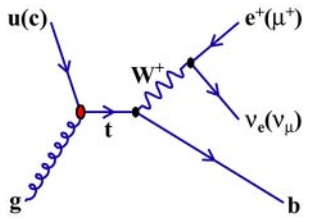

Fig. 2. – Leading-order Feynman diagram of non-SM production of a single top quark via the FCNC process u(c)+g $\to$ t [2].

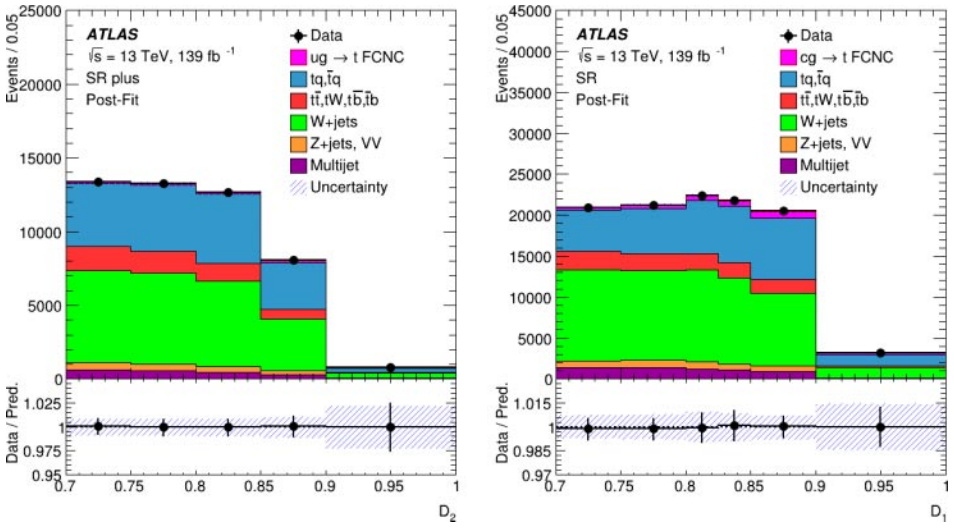

Fig. 3. – Left: The NN discriminant D_1 of the cgt search is shown with the post-fit normalisation applied to the stacked histograms of the different hard-scattering processes. The histogram shows a zoomed-in view of the high discriminant region between 0.7 and 1.0. Right: The NN discriminant D_2 of the ugt search is shown with the post-fit normalisation applied to the stacked histograms of the different hard-scattering processes. A zoomed-in view of the high discriminant region between 0.7 and 1.0 is displayed in the positively charged lepton channel [2].

products of a singly produced top quark. The background contributions with prompt leptons are modelled by MC simulation and normalized to their expected cross section except the W+jets normalization that is extracted from the fit. The multijet background is modelled from MC simulation for electrons and from collision data for muons. The rate of the multijet background is determined in a data-driven way by fitting the E_T^{miss} distribution for events with an electron and the $m_T(W)$ distribution for events with a muon.

Neural networks based on kinematic variables differentiate between events from the two signal processes, u+g→t and c+g→t, and events from background processes. One discriminant (D_1) was used for the cgt analysis and the negative lepton channel of the ugt analysis shown in fig. 3 (left). The other discriminant (D_2) was used for the positive lepton channel of the ugt analysis shown in fig. 3 (right).

The measured data are consistent with the background-only hypothesis, and limits are set on the production cross-sections of the signal processes: $\sigma(u + g \to t) \times B(t \to Wb) \times B(W \to l\nu) < 3.0$ pb and $\sigma(c+g\to t)\times B(t\to Wb)\times B(W\to l\nu) < 4.7$ pb at the 95% CL, with $B(W\to l\nu) = 0.325$ being the sum of branching ratios of all three leptonic decay modes of the W boson.

Based on the framework of an effective field theory (EFT), the cross-section limits are translated into limits on the strengths of the tug and tcg couplings occurring in the theory: $|C_{uG}^{ut}|/\Lambda^2 < 0.057$ TeV^{-2} and $|C_{uG}^{ct}|/\Lambda^2 < 0.14$ TeV^{-2}. These bounds correspond to limits on the branching ratios of FCNC-induced top-quark decays: $B(t\to u+g) < 0.61 \times 10^{-4}$ and $B(t\to c+g) < 3.7 \times 10^{-4}$.

Common selections		
Exactly 3 leptons with $p_{\mathrm{T}}(\ell_1) > 27\,\mathrm{GeV}$ ≥ 1 OSSF pair, with $\lvert m_{\ell\ell} - m_Z \rvert < 15\,\mathrm{GeV}$		
SR1	SR2	
≥ 2 jets	1 jet	2 jets
1 b-jet	1 b-jet	1 b-jet
–	$m_{\mathrm{T}}(\ell_W, \nu) > 40\,\mathrm{GeV}$	$m_{\mathrm{T}}(\ell_W, \nu) > 40\,\mathrm{GeV}$
$\lvert m^{\mathrm{reco}}_{j_a \ell\ell} - m_t \rvert < 2\sigma_{t_{\mathrm{FCNC}}}$	–	$\lvert m^{\mathrm{reco}}_{j_a \ell\ell} - m_t \rvert > 2\sigma_{t_{\mathrm{FCNC}}}$
–	$\lvert m^{\mathrm{reco}}_{j_b \ell_W \nu} - m_t \rvert < 2\sigma_{t_{\mathrm{SM}}}$	$\lvert m^{\mathrm{reco}}_{j_b \ell_W \nu} - m_t \rvert < 2\sigma_{t_{\mathrm{SM}}}$

Fig. 4. – Overview of the requirements applied for selecting events in the signal regions. OSSF is an opposite-sign same-flavor lepton pair [3].

3. – Search for FCNC couplings between the top quark and the Z boson with the ATLAS detector

This search targets both events where a single top quark is produced as gq→tZ (with q=u,c) and top-quark pair events, with one top quark decaying through the t→qZ channel [3]. The analysis selects events with three leptons (electrons or muons), a b-tagged jet, possible additional jets and missing transverse momentum. Two separate signal regions (SRs) are defined, targeting the two processes: SR1 targets FCNC processes in $t\bar{t}$ decays while SR2 targets FCNC processes in single top-quark production. The SRs share common selections for the leptons and they differ in the top-quark reconstruction and the jet multiplicity requirements as shown in the table in fig. 4. The main background contributions are $t\bar{t}Z$ and diboson processes plus heavy flavor jets (VV+HF). Several control regions are defined in order to check the background contributions. Multivariate discriminants are used to distinguish the signal and background events.

The data are consistent with the background-only hypothesis and 95% CL limits on the branching ratios are set. These are 6.2×10^{-5} (13×10^{-5}) for t→Zu (t→Zc) for a left-handed coupling, and 6.6×10^{-5} (12×10^{-5}) in the case of a right-handed coupling.

4. – Search for new physics using top quark pairs produced in associated with a boosted Z or Higgs boson in EFT with the CMS detector

The first search of new physics with $t\bar{t}Z$ and $t\bar{t}H$ events with a boosted Z/H boson using EFT at the LHC is presented [4]. These processes are particularly interesting, as they provide direct access to the couplings of the top quark to the Z and Higgs bosons. This analysis targets the $Z/H \to b\bar{b}$. A deep multi-classifier neural network is trained to differentiate signal from the main background contributions, $t\bar{t} + b\bar{b}$. Templates binned according to DNN score and reconstructed Z/H candidate mass are built to measure the signal strengths of boosted $t\bar{t}Z$ and $t\bar{t}H$ processes.

Upper limits are placed on the differential cross sections as functions of the Z or Higgs boson transverse momentum as shown in fig. 5.

EFT effects cause large deviations from the SM production of $t\bar{t}Z$ and $t\bar{t}H$ in the boosted regime. Eight possible dimension-six operators are added to the standard model Lagrangian and their corresponding coefficients are constrained via a fit to the data providing competitive constraints on top+EW EFT Wilson coefficients (WC) in previously unexplored phase space. The results are shown in fig. 6.

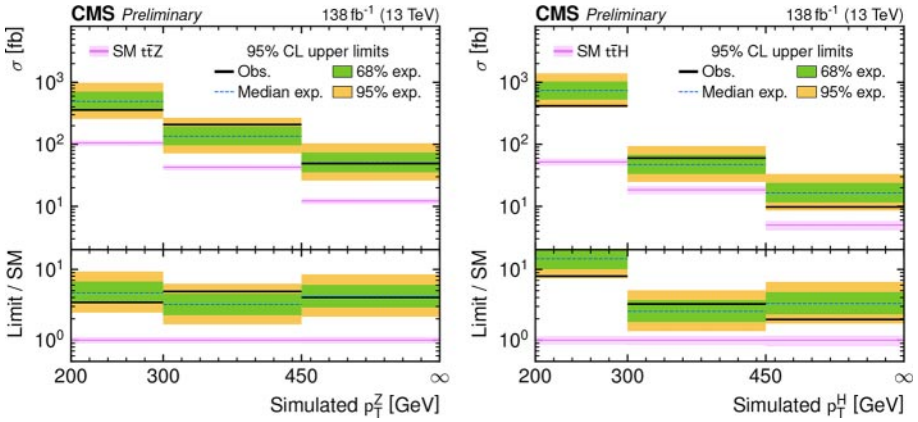

Fig. 5. – Observed and expected 95% CL upper limits on the $t\bar{t}Z$ (left) and $t\bar{t}H$ (right) differential cross sections as a function of Z and Higgs boson p_T. The green and yellow bands show the expected 95% CL upper limits while the black lines represent the observed 95% CL upper limits. The magenta lines show the SM predicted differential cross section PDF plus α_s and QCD scale uncertainties [4].

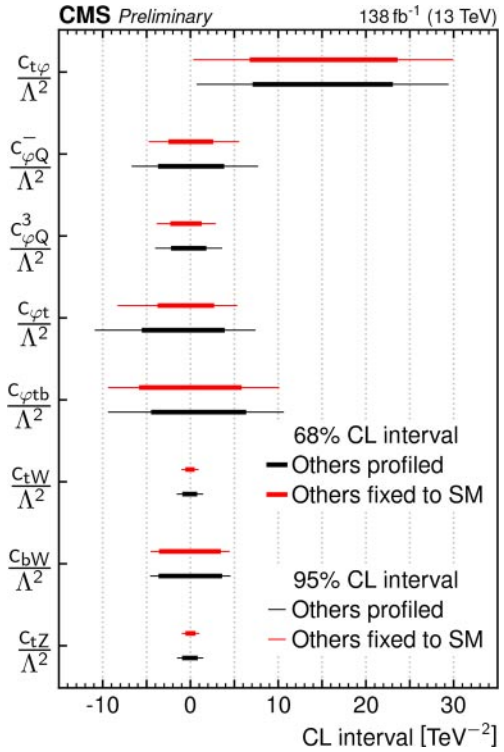

Fig. 6. – The observed 68 and 95% CL intervals for the WCs. The intervals are found by scanning over a single WC while either treating the other seven as profiled, or fixing the other seven to the SM value of zero [4].

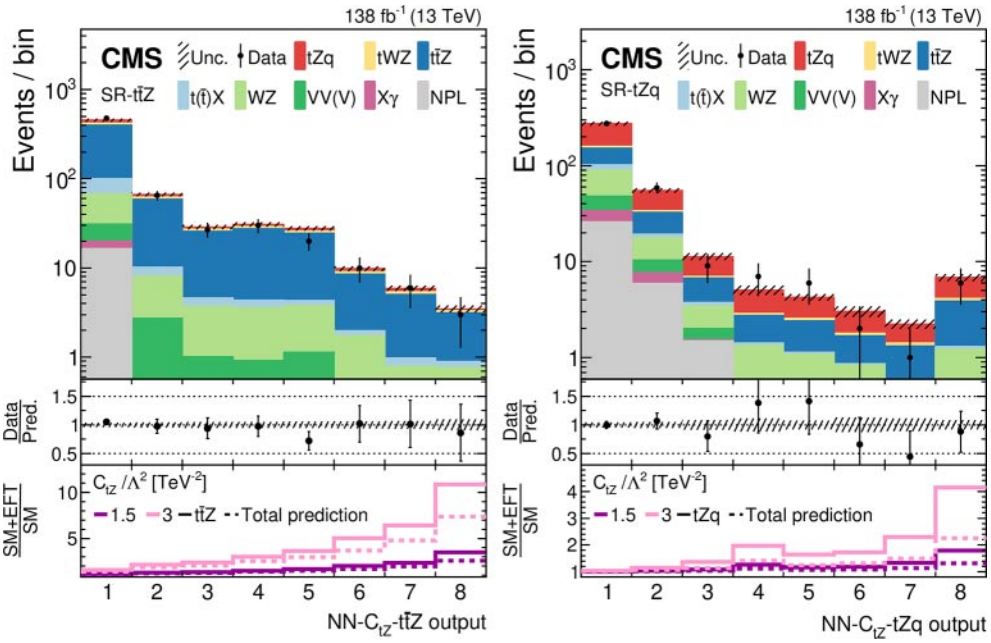

Fig. 7. – Post-fit data-to-simulation comparisons for the distributions used in the SR-ttZ (left) and SR-tZq (right), for the 1D fit to c_{tZ}. The middle panels display the ratios of the observed event yields to their post-fit expected values. For each region, the lower panel shows the change of the event yield in each bin with respect to the SM post-fit expectation for two benchmark EFT scenarios, both for the main signal process in the region (thick lines) and for the total prediction (dashed lines) [5].

5. – Probing EFT operators in the associated production of top quarks with a Z boson in multilepton final states with the CMS detector

The search for new top quark interactions performed within the framework of an EFT theory using the t($\bar{t}$)Z events in multilepton final states is presented with the full Run 2 data [5]. Five dimension-six operators modifying the electroweak interactions of the top quark are considered. Machine-learning techniques, NN, are used to enhance the sensitivity to effects arising from these operators as the ones presented in fig. 7. For the first time machine-learning techniques that account for the interference between EFT operators and the SM amplitude have been used in an LHC analysis.

All five Wilson coefficients are simultaneously fit to data in six categories and 95% CL intervals are computed, see the table in fig. 8.

6. – Measurement of the inclusive and differential ttγ cross sections in the dilepton channel and EFT interpretation with the CMS detector

The production cross section of a top quark pair in association with a photon is measured in pp collisions in the decay channel with two oppositely charged leptons using 138 fb^{-1} of data recorded by the CMS experiment is presented [6]. The inclusive cross section is extracted with a profile likelihood fit to the transverse momentum distribution of the reconstructed photon, see fig. 9. An inclusive cross section of

WC/Λ^2	95% CL confidence intervals			
$[TeV^{-2}]$	Other WCs fixed to SM		5D fit	
	Expected	Observed	Expected	Observed
c_{tZ}	$[-0.97, 0.96]$	$[-0.76, 0.71]$	$[-1.24, 1.17]$	$[-0.85, 0.76]$
c_{tW}	$[-0.76, 0.74]$	$[-0.52, 0.52]$	$[-0.96, 0.93]$	$[-0.69, 0.70]$
$c^3_{\varphi Q}$	$[-1.39, 1.25]$	$[-1.10, 1.41]$	$[-1.91, 1.36]$	$[-1.26, 1.43]$
$c^-_{\varphi Q}$	$[-2.86, 2.33]$	$[-3.00, 2.29]$	$[-6.06, 14.09]$	$[-7.09, 14.76]$
$c_{\varphi t}$	$[-3.70, 3.71]$	$[-21.65, -14.61] \bigcup [-2.06, 2.69]$	$[-16.18, 10.46]$	$[-19.15, 10.34]$

Fig. 8. – Expected and observed 95% CL confidence intervals for all WCs. The intervals in the first and second columns are obtained by scanning over a single WC, while fixing the other WCs to their SM values of zero. The intervals in the third and fourth columns are obtained by performing a 5D fit in which all five WCs are treated as free parameters [5].

173.5 ± 2.5 (stat) ± 6.3 (syst) fb is measured in a signal region with at least one jet coming from the hadronization of a bottom quark and exactly one photon with transverse momentum above 20 GeV.

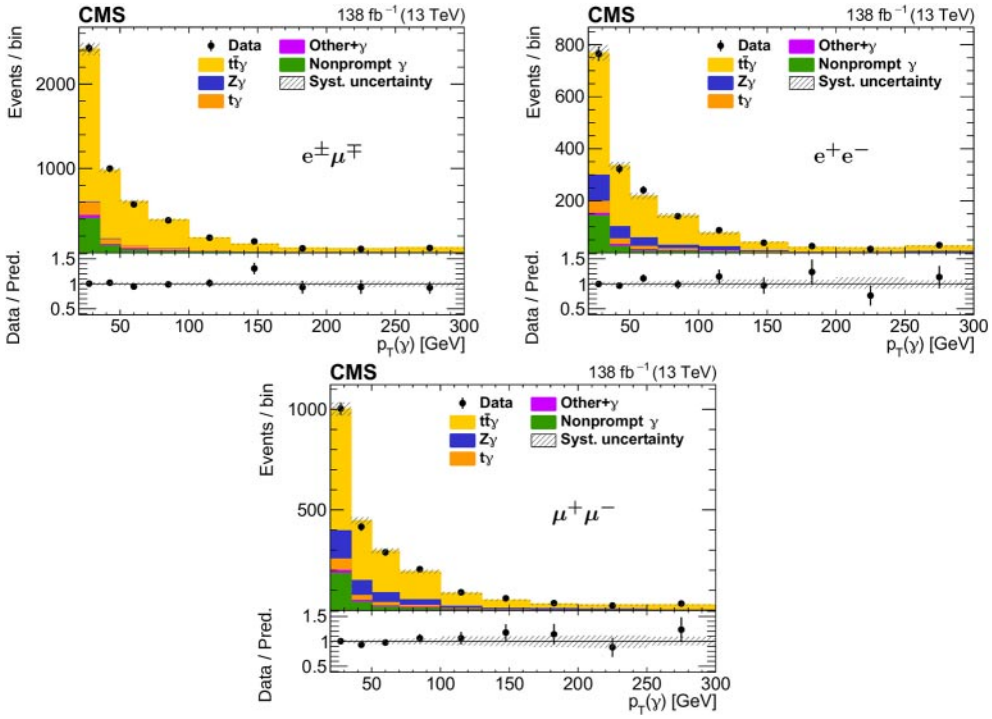

Fig. 9. – The observed (points) and predicted (shaded histograms) event yields as a function of the reconstructed photon p_T after applying the signal selection, for the $e^{\pm}\mu^{\mp}$ (upper left), $e^{-}e^{+}$ (upper right), and $\mu^{-}\mu^{+}$ (lower) channels, after the values of the normalizations and nuisance parameters obtained in the fit to the data are applied. The vertical bars on the points show the statistical uncertainties in data, and the hatched bands the systematic uncertainty in the predictions. The lower panels of each plot show the ratio of the event yields in data to the predictions [6].

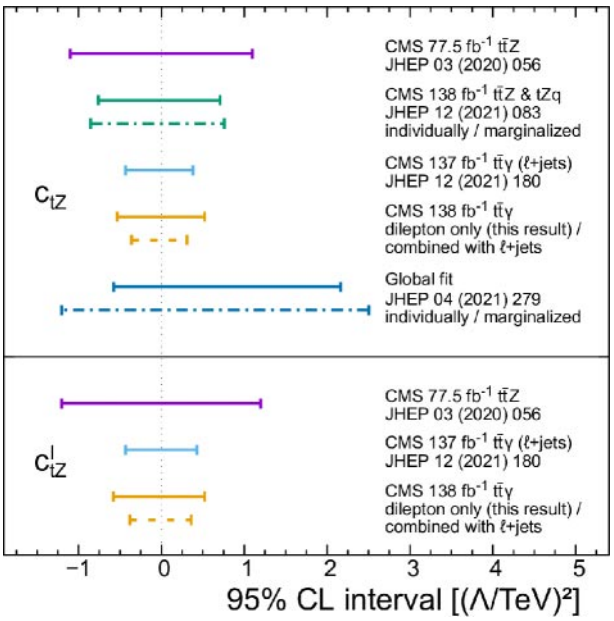

Fig. 10. – Comparison of observed 95% CL intervals for the Wilson coefficients c_{tz} (upper panel) and c^I_{tz} (lower panel) [6].

Differential cross sections are measured as a function of several kinematic observables of the photon, leptons, and jets and compared to SM predictions showing good agreement. Measurements are also interpreted in the SM EFT framework. Limits are found on the c_{tz} and c^I_{tz} Wilson coefficients describing the modifications of the $t\bar{t}Z$ and $t\bar{t}\gamma$ interaction vertices as presented in fig. 10.

7. – Summary

The large amount of LHC data recorded up to date allows probing very rare standard model processes, processes with very small production cross sections and even measure their differential cross sections. Rare processes with top quarks are sensitive to beyond the SM interactions and searches of flavor-changing neutral-current couplings are performed. In addition, first searches are carried out within the framework of an effective field theory. So far all results are in good agreement with SM predictions.

REFERENCES

[1] ATLAS Collaboration, ATLAS-CONF-2022-003, https://cds.cern.ch/record/2802004.
[2] ATLAS Collaboration, *Eur. Phys. J. C*, **82** (2022) 334.
[3] ATLAS Collaboration, ATLAS-CONF-2021-049, https://cds.cern.ch/record/2781174.
[4] CMS Collaboration, CMS-PAS-TOP-21-003, https://cds.cern.ch/record/2802060.
[5] CMS Collaboration, *JHEP*, **12** (2021) 083.
[6] CMS Collaboration, *JHEP*, **05** (2022) 091.